Estimating a nonradial vignetting shape

Dorotea Potoč, Davor Petrinović
University of Zagreb
Faculty of Electrical Engineering and Computing
dorotea.potoc@fer.hr, davor.petrinovic@fer.hr

***Abstract*—Vignetting is a phenomenon characterized by a decrease in illumination towards the edges of an image. This effect is typically represented by a radially symmetrical model, however, this paper aims to demonstrate a non-radial model of vignetting and estimate its shape. To accomplish this, a synthetic image was created and the angular vignetting shape has been modeled as a sum of harmonics. The magnitudes and amplitudes of these harmonics were obtained and used to construct the desired angular vignetting shape. Once the synthetic image with the modeled vignetting shape and added noise was created, it was used as input into a function for vignetting estimation. Also, the inputs have been a fixed vignetting center and different initial values of harmonics' magnitudes and phases. With that inputs, despite the level of the noise, we have successfully estimated vignetting function by non-linear optimization. The function has attempted to determine the original harmonics' used to create the vignetting angular shape. When the vignetting model is calculated, we removed it in order to get a homogeneous image. While it may be difficult to obtain the exact original values of the harmonics', the shape can be estimated with a high level of accuracy. The paper shows that highly accurate models can be estimated for a lower number of angular harmonics, with a residual gain error standard deviation of less than 0.03%. Even in the presence of 5dB noise in the images, the gain error standard deviation remains below 3%, as long as proper parameter initialization is performed prior to optimization.**

***Keywords*—vignetting, non-radial model, vignetting correction, optimization**

I. Introduction

Vignetting is a photometric phenomenon in which the brightness of an image decreases towards its periphery, relative to its center. The cause of vignetting can be due to limitations in camera and lens design, such as the aperture value, or the geometric distortion of oblique light beams. It can introduce inaccuracies in computer vision algorithms that rely on precise intensity data. Vignetting correction techniques range from commercial to non-commercial solutions, but the majority assume radial distribution [1], [2], leading to potential inaccuracies if the vignetting is actually non-radial. The degree of vignetting is influenced by factors such as lens, aperture, and exposure, making automatic correction challenging [3].

The characteristics of the lens and its aperture determine the degree of vignetting. Natural vignetting occurs due to the cosine fourth law of illumination fall-off, which states the decrease in light is proportional to the fourth power of the cosine of the angle between peripheral lens rays and the optical axis. The aperture, or diaphragm, regulates the amount of light reaching the sensor and controls the f-stop, a logarithmic measure of the ratio of maximum to minimum intensity [4].

Vignetting has four different types: optical vignetting is a lens-based phenomenon of gradual darkening in images that are more prominent at wider apertures. It can be corrected by reducing the aperture size [5]. Natural vignetting is caused by the light reaching the sensor at different angles, particularly with wide-angle lenses, and is a result of the cosine fourth law of light fall-off [6]. It cannot be corrected with aperture adjustment but can be compensated through filters or image processing. Mechanical vignetting results from physical obstruction of light by filter rings, hoods, or other objects and is less noticeable with wider apertures and zoom lenses. Pixel vignetting is due to lower illumination of corner pixels compared to center pixels, which is a result of the flat construction of image sensors and the angle of the light impinging on the sensor. It can be reduced by using micro-lenses on the sensor and perpendicular angles, though it cannot be eliminated entirely [7], [8].

The vignetting can be reduced using radial graduated neutral density filters or by post-processing methods. Some cameras have a built-in vignetting correction for JPEG images, but not for RAW images. Image processing can be used to enhance images and correct vignetting, but various lens-related factors such as angle of incidence, chief ray angle (CRA) misalignment, and natural vignetting must be considered. Correction methods for RAW images require specialized software. Image processing methods can also enhance the quality of the image. Most causes of vignetting can be reduced by decreasing the lens aperture by 2 f-stops, or through the use of a telecentric lens that produces uniform illumination of the image plane. Mechanical vignetting can be reduced by using longer focal lengths, using a telecentric lens, or using flat field correction.

Any optical system consisting of multiple lenses can cause non-radial vignetting. This occurs because lenses typically have around 20 elements, and their misalignment with the optical axis can lead to non-radial vignetting. Specifically, due to the mechanical and lens imperfections and for lenses with variable focus. Even high-end lenses may not have a perfect internal construction, which can

This work was supported in part by the Croatian Science Foundation under Project IP-2019-04-6703 and DOK-2021-02-6215 and in part by the European Regional Development Fund under Grant KK.01.1.1.01.0009 (DATACROSS). Any opinions, findings, and conclusions to recommendations expressed in this material are those of the authors and do not necessarily reflect the views of the Croatian Science Foundation.

lead to this phenomenon. For example, there is one lens that has 17 elements divided into 12 groups [9], it is a very high-rated lens, but can still cause this phenomenon.

Non-radial vignetting can also occur in scenarios where the illumination is not sufficiently homogenous.

II. Related works

Vignetting correction methods aim to eliminate the darkening of image corners caused by the vignette effect. These techniques can be broadly divided into two groups: those that use a reference image and those that do not. The former group relies on a reference image to determine a vignetting function, which is obtained by approximating the function with parametric models.

Physically-based models within this group require detailed knowledge of camera lens parameters and can be challenging to implement [10], [11]. Single-image [12], [13], [14] and image sequence methods [15], [16], [17], [18] within this group estimate vignetting by minimizing an objective function with the assumption that vignetting is a radial function. These methods often require additional image processing techniques, such as image segmentation [1].

The effectiveness of methods that use a single image to estimate a vignetting function depends on the precision of localization of corresponding pixels and usually use additional image processing methods, eg. image segmentation. Most single-image correction methods do not require prior knowledge of the vignette model or optical system and can be achieved through: radial and tangential gradient analysis [19], Gaussian quadric fitting [20], and estimation of correction factors at each pixel position [21]. Some of these methods also take into consideration pupil aberration and the symmetric distribution of the radial gradient [22], [23]. In most cases, all compared images require an acquisition in the same scene conditions and any change in the scene may influence the outcome vignetting function. The effectiveness of these methods strongly depends on the uniformity of scene illumination.

In the image sequence method, they use a set of not entirely overlapping images of the same reference scene to calculate vignetting function. It is done by minimizing the objective function which depends on the differences between values of corresponding pixels in different images, which represent the same scene point. Multiple-image correction techniques may require prior knowledge of the optical system or vignetting model and use information from multiple images to estimate a vignetting model. These methods can be model-based or otherwise utilize techniques such as wavelet decomposition and hyperbolic function approximation

Methods that do not use reference images are based on flat-field correction and assume a reference vignetting image that represents a uniformly illuminated surface. There can be used different types of vignetting models, such as 2D polynomial [15], [24], [25], exponential 2D polynomial [24], smooth non-iterative local polynomial [26], radial polynomial [27], hyperbolic cosine [28], and Gaussian function [29]. Most models represent a radial model, but there are only few methods that cover non-radial models, and are easy to use.

Type of Methods		Reference
With reference image		
Physically based model		
	Natural, optical, pixel	[10], [11]
Single image:		[12] - [14]
	Radial and tangential gradient analysis	[19]
	Gaussian quadric fitting	[20]
	Estimation of correction factors	[21],
	Non-radial methods	[3], [30], [31]
Image mosaic:		
	Model-based	[17] , [18]
	Wavelet decomposition	[2]
	Hyperbolic function approximation	[15]
Without reference image		
Flat field:		
	2D polynomial	[24], [25]
	Exponential 2D polynomial	[24]
	Smooth non-iterative local polynomial	[26]
	Radial polynomial	[27]
	Hyperbolic function	[28]
	Gaussian function	[29]

TABLE I: Type of methods for vignetting correction

A. Non-radial vignetting correction methods

Non-radial vignetting correction methods are mostly done as single-image vignetting correction. There are a few methods that deal with this type of vignetting.

Non-radial vignetting correction described in [3] is based on a local parabolic model of vignetting. This algorithm includes compensation for non-uniform scene luminance. The method shows better results on artificial images than on natural ones. The usual quality metrics for luminance compensation accuracy are MAE and RMSE measures.

Another approach, Deformable Radial Polynomial (DRP) model combines the simplicity of the commonly used radial polynomial(RP) model with the universality of more complex methods. This model uses a distance transformation and minimization method to match the radial vignetting model to the non-radial vignetting of the analyzed lens-camera system and can give better results than the RP model [30].

An alternative approach of local fitting of the vignetting model to the measure data [31] is based on the local polynomial model in which the order of the polynomial is a parameter of the model and allows to better fit the model to the real vignetting of camera-lens systems.

Our preliminary results are not yet comparable to the results obtained by existing methods. Further research and optimization are necessary to fully evaluate the potential of the proposed approach.

III. Proposed non-radial model of vignetting

Radial vignetting shown in Figure 1 is the most widely recognized form of vignetting and has been well studied, leading to the development of numerous correction algorithms that take its radial shape into account. However, non-radial vignetting, shown in Figure 2, is a more complex form of vignetting that is more difficult to quantify and

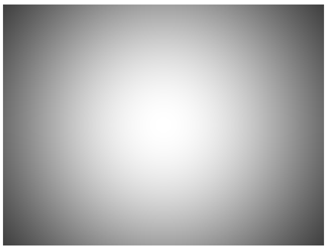

Fig. 1: Radial model of vignetting [32]

correct. This is due to the lack of a uniform and systematic pattern in the reduction of brightness or saturation across the image plane. Non-radial vignetting correction methods are still an active area of research in the field of image processing.

Fig. 2: Example of a non-radial model of vignetting

The general form of vignetting can be expressed mathematically as a function of the normalized radius, as shown in equation 1.

$$V = f(R') \tag{1}$$

In the proposed model, in the equation 2, the normalized radius is defined by multiplying the actual radius by an angular dependent factor k(θ) that accounts for the desired non-radial shape of the vignetting.

$$R' = \frac{R}{maxR} \cdot k(\theta) \tag{2}$$

The factor k(θ) is a function of the polar angle, θ, and allows for the creation of a non-uniform reduction of image brightness or saturation across the image plane. The non-radial form of vignetting can be used to model more complex forms of vignetting beyond the traditional radial model, allowing for greater control over the shape and intensity of the vignetting effect.

For a radially symmetric vignetting model, the factor k(θ) is a constant, meaning that the reduction in image brightness or saturation is uniform in all directions. In contrast, for a non-radially symmetric vignetting model, the factor k(θ) varies as a function of the polar angle, θ, which allows for the creation of non-uniform vignetting patterns that fall off at different rates in different directions. The larger the value of k(θ), the more rapid the reduction of brightness or saturation in that direction. By modeling vignetting in this manner, it is possible to create more complex and nuanced vignetting effects.

$$k(\theta) = 1 + \sum_{n=1}^{Nh} (ma_i \cdot \cos(\arctan(\frac{y - y_0}{x - x_0}) \cdot i + an_i) \tag{3}$$

The proposed angular term k(θ) of the non-radial vignetting model is determined as a simple sum of the harmonics, as expressed in equation 3 where (x, y) is the pixel position in the frame, (x_0, y_0) is the center of the shifted vignetting model, and R is the euclidean distance of these two points. Such a definition ensures natural periodicity with the period of 2π, thus achieving the angular smoothness of the model. In this equation, ma_i represents the magnitude and an_i represents the angle of each harmonic term. The sum of these harmonics results in the final expression for angular dependent normalized radius R'. The proposed approach allows for a flexible parametric representation of the vignetting effect and the ability to control the shape and intensity of the vignetting by adjusting the magnitude and angle of each harmonic term. By combining multiple harmonics, it is possible to create complex and non-uniform vignetting patterns that cannot be represented by simple radial models.

IV. Proposed method of non-radial vignetting correction

A. *Synthetic image of non-radial model*

Since such a model has not been studied in the literature so far, before comparing it to other models and before its validation on real-world images it was necessary to establish the feasibility of model estimation from synthetic images with given model parameters. This represents the main research objective presented in this paper.

To validate the vignetting correction function, a synthetic image, shown in Figure 3 was created as follows: 1) a homogeneous gray image was established as the background to simulate the uniform part of the night sky glow, 2) white pixels simulating stars were added to the constant value of the image, 3) the described non-radial vignetting model was then applied to the image, and 4) Poisson noise was applied to the image to simulate the realistic noise present in images captured by cameras. The presence of noise can make it difficult to accurately estimate the form of vignetting, potentially leading to discrepancies between the estimated and actual vignetting models, especially when the sensor's response to sky glow intensity is of a similar magnitude to the expected noise level. Therefore, it is essential to consider the impact of noise when estimating the vignetting correction, as it can further exacerbate the vignetting correction problem.

B. *Function for vignetting correction*

The function operates based on the principle of pixel sensing and attempts to identify the shape of vignetting by searching for areas where the function assumes the same intensity values. In simple radial models, search is performed along contour lines of equal intensity which are

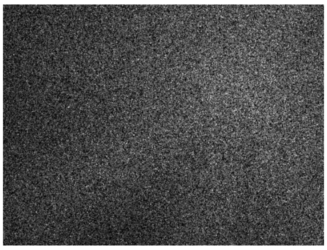

Fig. 3: Example of synthetic image with non-radial vignetting, Nh = 9

represented by concentric circles. Based on the proposed angular model from equation 3 with assumed harmonics values, the contour lines become non-circular as shown in Figure 4 for the same example from Figure 3.

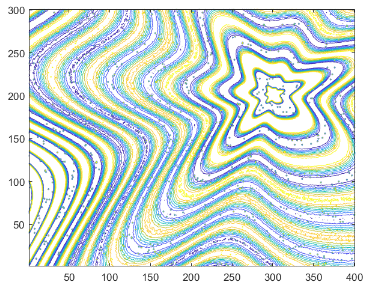

Fig. 4: Contour lines of non-circular model, Nh = 9

The radial cut of the normalized vignetting function f(R') is then determined by averaging across all angles θ. Introducing such angular dependent scaling of radial distance to the vignetting model's center is equivalent to the image frame spatial distortion in which the vignetting of the original undistorted image would be a simple radial model of the normalized radius R'. The original and distorted frames are shown in Figure 5.

Ideally, the vignetting estimation function shall result with the optimal set of parameters: model center (x_0,y_0), angular model harmonics (ma_i and an_i), and the normalized radial cut function V(R'), using the non-linear optimization for the chosen loss function. Since this is a non-trivial problem we have experimented with a different kind of parameter initialization which affect the final solution.

The inputs to the optimization function are thus initial magnitudes and phases of harmonics and the vignetting center point which is either assumed as a free optimization variable as well or is fixed to the actual known position to simplify the problem. The radial cut function is also modeled as a harmonic function of the normalized radius R' with the chosen number of radial harmonics (20 in all our experiments). The parameters of this averaged radial harmonic model are always determined as an optimal solution for the current parameters of the assumed angular vignetting model k(θ).

In this paper, we will present the estimation results for the fixed center position in order to validate the possibility of estimating an accurate angular model for such a simplified case.

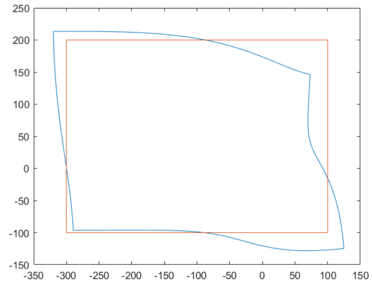

Fig. 5: Distorted shape of the frame due to angular dependent radial scaling, Nh=2

The estimation process is inherently nonlinear, rendering the task of identifying the optimal solution intractable through analytical methods. A reliable estimate of the model will be obtained if the application of the reciprocal model to the image results in a uniform brightness across the entire frame, with minimal variations. To minimize these variations in consideration of the model's parameters, numerical optimization was performed in Matlab utilizing the fminunc function, as well as a similar function developed within our department.

V. Experiments and results

Experimental verification of vignetting estimation and compensation was done on the synthetic image (300x400 pix) with x_0 = 200, y_0 = 150. In order to evaluate our estimation methodology, the number of harmonics of the angular model was varied from the set Nh = {1, 2, 9}, so we can validate the estimation function behavior for a small number of harmonics, as well as a larger value. To verify the robustness of the final estimation result to the proper parameter initialization, optimization was initialized with the scaled values of the ideal harmonics magnitudes and phases which were used for the image synthesis. The same scalar scaling factor α was used for all initial parameters, which was chosen from the set α = {1, 0.7, 0.4, 0.2, 0, -1}. Every experiment was performed for the noise-free synthetic image as well as for the Poisson corrupted image with an SNR of 20dB and 5 dB. The normalized radial cut function of the synthetic image was chosen as V(R') = tan($\frac{\pi}{4}$ - $\frac{\pi}{8}$ $\frac{R'}{maxR'}$), such that V(0) = 1, and V(maxR') = 0.4142.

For the trivial scale factor α = 1, initial optimization parameters were identical to the parameter set used for synthesis which truly minimizes the objective function so this case represents the baseline for comparison.

A. Evaluation metrics

The success of the vignetting estimation and compensation was measured by two factors: standard deviation (std) of the residual gain variation to the unit value and the percentage of valid pixels (valid) whose gain variation is within +/-3std (to account for inevitable outliers). The robust estimate of the std was used to establish the validity threshold to account for heavy-tailed gain error distribution. Therefore, both values must be considered when interpreting and comparing the experimental results.

B. Experiments with noise-free images

The estimation results of compensating noise-free images are presented in Figures 6, 7, and 8 for scaling factor α = 0.4. The correction is demonstrated to be very successful with minimal deviation from the unit value of less than 1 permille relative gain variation for Nh = 1. Residual radial fringes are caused by the mismatch between the radial cut model used for the synthesis (tan) and the non-parametric harmonic model which is used in the estimation to account for the arbitrary radial cut shape. The angular model error can be observed for Nh = 9 as angular zoning combined with radial fringes, but the error is still within 1% of the ideal flatness.

The numerical simulation results for all three choices of Nh are presented in Tables II to IV. It can be observed from Table II that for an angular model with a single harmonic, the true model parameters (ma_1, an_1) can be easily resolved for all positive values of scaling factor α. In table III, for a model with 2 harmonics the true parameter values are restored for scaling factor $\alpha \geq 0.7$, while for the most complex model with Nh = 9, most of the parameters are restored to the true value for scaling factor $\alpha \geq 0.7$ (Table IV). However, for smaller or negative scaling of the initial parameters, in all 3 cases, the minimization function becomes trapped in an alternative minimum and approaches its closest values which are not the global minimum.

The reconstruction accuracy of the compensated synthetic image is also presented in Tables II, III and IV in the last three rows through the percentage of valid pixels and corresponding standard deviation of the residual gain variation. The last row displays the required number of optimization iterations, showing that a more complex model as well as poor initialization increases its value. Similar behavior is observed for the compensation accuracy demonstrating the importance of appropriate initialization.

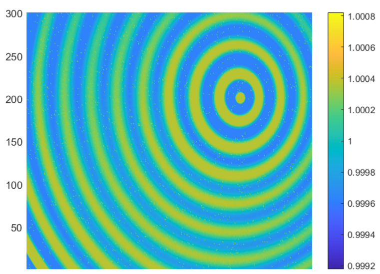

Fig. 6: Residual gain variations for noise-free image, Nh=1, α = 0.4

C. Testing images with SNR = 20dB

The estimation results of the vignetting correction in the image with the signal-to-noise ratio (SNR) of 20 dB is illustrated in Figure 9 for α = 0.7. The compensation error

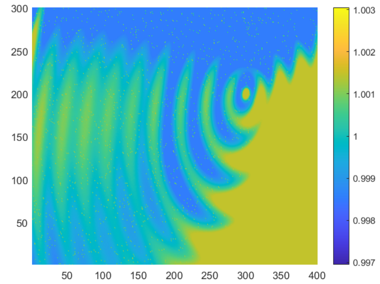

Fig. 7: Residual gain variations for noise-free image, Nh=2, α = 0.4

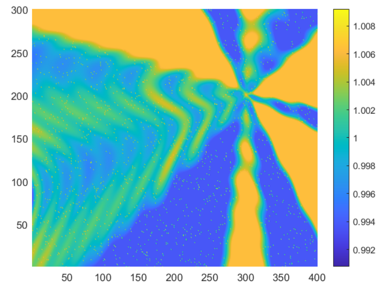

Fig. 8: Residual gain variations for noise-free image, Nh=9, α = 0.4

param	true\\α	1	0.7	0.4	0.2	0	-1
ma_1	0.0799	0.0799	0.0798	0.0798	0.0798	0.0791	-0.0798
an_1	-0.0666	-0.0666	-0.0680	-0.0676	-0.0687	-0.0689	0.4330
valid %	-	99.200	99.099	99.153	99.151	99.114	99.164
std %	-	0.0306	0.0328	0.0316	0.0350	0.0357	0.0306
Iter num	-	4	32	48	43	63	77

TABLE II: Values of the estimated parameters for scaled initialization for noise-less image, Nh = 1

param	true\\α	1	0.7	0.4	0.2	0	-1
ma_1	0.0986	0.0986	0.0690	0.1007	0.0795	0.1023	-0.2977
ma_2	0.1819	0.1819	0.1281	0.1971	0.2020	0.1680	-0.0327
an_1	0.1011	0.1011	0.0710	0.0567	0.0448	0.1433	-0.1894
an_2	-0.0703	-0.0703	-0.0503	-0.0728	-0.0779	-0.0672	0.2558
valid %	-	99.095	98.360	80.483	80.713	80.443	72.894
std %	-	0.0297	2.0874	0.1503	0.1690	0.1390	1.1579
Iter num	-	6	18	86	55	146	64

TABLE III: Values of the estimated parameters for scaled initialization for noise-less image, Nh = 2

param	true\\α	1	0.7	0.4	0.2	0	-1
ma_1	0.0466	0.0466	0.0340	0.0340	-0.0431	-0.0460	-0.0111
ma_2	0.1014	0.1014	0.0945	0.0641	0.0408	-0.0200	-0.0287
ma_3	0.0360	0.0360	0.0164	-0.0141	-0.0067	0.0510	0.0029
ma_4	0.1408	0.1408	0.1318	0.1154	0.1107	0.1673	-0.0404
ma_5	0.0895	0.0895	0.0700	0.0572	0.0046	-0.0206	-0.1819
ma_6	0.0176	0.0176	-0.0098	-0.0951	-0.0234	-0.0570	0.0644
ma_7	0.1566	0.1566	0.1570	0.1288	0.1703	0.1584	-0.0029
ma_8	0.0218	0.0218	0.0066	0.0425	0.0326	-0.0230	0.0970
ma_9	0.0366	0.0366	0.0524	0.0369	0.0652	0.0300	0.0191
an_1	0.4492	0.4492	0.3070	0.1696	0.1059	0.0706	-0.4483
an_2	0.2998	0.2998	0.2399	0.1314	0.1048	-0.0430	-0.2563
an_3	-0.4346	-0.4346	-0.3194	-0.1710	-0.0987	-0.1294	0.4460
an_4	-0.0787	-0.0787	-0.0655	-0.0658	0.0682	0.0265	0.1312
an_5	-0.2185	-0.2185	-0.1720	-0.1298	-0.0842	0.0072	0.1818
an_6	-0.4015	-0.4015	-0.2829	-0.1572	-0.0938	-0.0136	0.3269
an_7	-0.0884	-0.0884	-0.0911	-0.0400	-0.0771	-0.1028	0.1899
an_8	0.4547	0.4547	0.3243	0.1795	0.1059	0.0196	-0.4922
an_9	-0.0004	-0.0004	0.0294	0.0423	0.0244	-0.0105	-0.0235
valid %	-	98.301	80.421	76.681	68.514	69.574	69.040
std %	-	0.0388	0.2673	0.6437	0.2115	0.1508	0.2545
Iter num	-	20	360	303	451	534	565

TABLE IV: Values of the estimated parameters for scaled initialization for noise-less image, Nh = 9

is shown for Nh = 2, but similar results were obtained for

Nh = 1 and Nh = 9 as well. The correction is successful with the maximal deviation from the unit value of slightly above 1% gain error. Detailed results presented in Tables V to VII indicate that the correction is slightly worse than for the noise-free images. The percentage of compensated pixels drops rapidly for $\alpha \leq 0.7$, which gives even higher significance to proper parameter initialization. We can also observe that the higher number of angular harmonics requires a significantly larger number of iterations (e.g. Nh = 9).

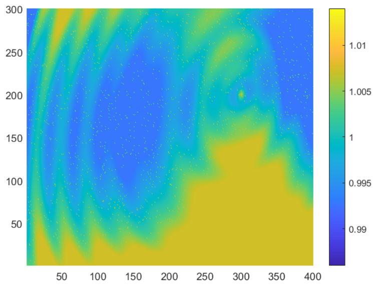

Fig. 9: Residual gain variations for image with SNR = 20dB, Nh=2, α = 0.7

param	true\\α	1	0.7	0.4	0.2	0	-1
ma_1	0.0799	0.0806	0.0559	0.0319	0.0169	0.0630	-0.0790
an_1	-0.0666	-0.0678	-0.0466	-0.0266	-0.0129	-0.0006	0.0683
valid %	-	97.356	99.962	99.940	99.824	99.838	98.691
std %	-	0.2433	0.6300	1.0944	1.3533	0.7765	2.0206
Iter num	-	9	4	4	12	21	17

TABLE V: Values of the estimated parameters for scaled initialization for image with SNR = 20dB, Nh = 1

param	true\\α	1	0.7	0.4	0.2	0	-1
ma_1	0.0986	0.1014	0.0704	0.0030	0.0262	0.0125	-0.1579
ma_2	0.1819	0.1828	0.1632	0.1899	0.0937	0.0628	-0.1050
an_1	0.1011	0.1005	0.0915	0.0650	0.0374	0.0002	-0.1451
an_2	-0.0703	-0.0677	-0.0995	-0.0596	0.0076	-0.0009	0.2053
valid %	-	99.164	99.319	100.000	99.946	99.988	100.000
std %	-	0.1641	0.7355	1.4962	3.8717	4.2820	2.6032
Iter num	-	27	37	47	22	24	44

TABLE VI: Values of the estimated parameters for scaled initialization for image with SNR = 20dB, Nh = 2

param	true\\α	1	0.7	0.4	0.2	0	-1
ma_1	0.0466	0.0472	0.0322	-0.0066	0.0154	0.0191	-0.0974
ma_2	0.1014	0.1008	0.0822	0.0153	0.0284	0.0567	-0.0727
ma_3	0.0360	0.0366	0.0286	-0.0184	-0.0146	0.0080	0.0617
ma_4	0.1408	0.1402	0.1103	0.0535	0.0548	0.0839	-0.0788
ma_5	0.0895	0.0894	0.0597	0.0686	0.0184	-0.0342	-0.1614
ma_6	0.0176	0.0175	-0.0049	-0.0446	-0.0224	-0.0768	0.0536
ma_7	0.1566	0.1562	0.1333	0.0207	0.0397	0.0992	-0.0030
ma_8	0.0218	0.0218	0.0563	0.0423	-0.0009	-0.0781	0.1066
ma_9	0.0366	0.0370	0.0470	0.0611	0.0372	0.0529	0.0238
an_1	0.4492	0.4490	0.3256	0.1566	0.0939	0.0032	-0.4687
an_2	0.2998	0.2996	0.2110	0.1821	0.0432	0.0210	-0.3730
an_3	-0.4346	-0.4345	-0.3093	-0.1735	-0.0892	0.0075	0.4193
an_4	-0.0787	-0.0777	-0.0630	-0.0323	-0.0222	0.0000	0.0955
an_5	-0.2185	-0.2181	-0.1700	-0.0872	-0.0577	0.0335	0.1729
an_6	-0.4015	-0.4015	-0.2704	-0.1629	-0.0944	-0.0348	0.3874
an_7	-0.0884	-0.0882	-0.0652	-0.0586	-0.0371	-0.0269	0.0878
an_8	0.4547	0.4552	0.3213	0.2018	0.0806	0.0102	-0.4813
an_9	-0.0004	-0.0004	0.0075	-0.0063	-0.0041	0.0115	-0.0391
valid %	-	99.141	91.550	98.643	99.827	97.293	95.299
std %	-	0.2548	0.9074	3.2596	4.1844	3.0358	1.7616
Iter num	-	81	105	111	85	184	295

TABLE VII: Values of the estimated parameters for scaled initialization for image with SNR = 20dB, Nh = 9

D. *Correction of low SNR images*

For the same initial scaling of α = 0.7, the optimization result of the vignetting correction of the low SNR image (SNR = 5 dB) is illustrated in Figure 10 for Nh = 2. The values shown in Tables VIII to X demonstrate that the results are worse than those obtained from images with a higher SNR, or those of the noise-free images, yet the vignetting function can still be approximately reconstructed with magnitudes and angles affected by the high noise level. It is observed that the smaller the number of harmonics, the easier it is to attain desired results, as the model depends on fewer free parameters. Additionally, it can be seen that even for such a high noise level, the percentage of the correctly compensated pixels is in the range of 97-99% with the residual std of around 2% gain error for $\alpha \geq 0.7$. The error clearly increases with poorer initialization.

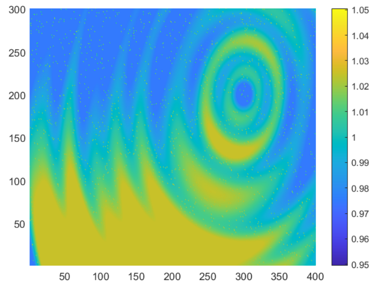

Fig. 10: Residual gain variations for image with SNR = 5dB, Nh=2, α = 0.7

param	true\\α	1	0.7	0.4	0.2	0	-1
ma_1	0.0799	0.0799	0.0559	0.0329	0.0160	0.0023	-0.0800
an_1	-0.0666	-0.0666	-0.0466	-0.0264	-0.0133	0.0004	0.0751
valid %	-	96.567	97.386	97.969	98.568	99.030	99.596
std %	-	1.2126	1.3729	1.6930	2.0619	2.2066	2.4473
Iter num	-	4	4	12	4	17	20

TABLE VIII: Values of the estimated parameters for scaled initialization for image with SNR = 5dB, Nh = 1

param	true\\α	1	0.7	0.4	0.2	0	-1
ma_1	0.0986	0.1006	0.0683	0.0394	0.0204	-0.0021	-0.0994
ma_2	0.1819	0.1825	0.1270	0.0728	0.0369	0.0010	-0.1819
an_1	0.1011	0.1011	0.0712	0.0404	0.0203	0	-0.1010
an_2	-0.0703	-0.0669	-0.0474	-0.0281	-0.0135	0	0.0698
valid %	-	96.961	99.742	99.857	99.944	100.000	99.998
std %	-	0.8132	2.3364	3.9619	4.7796	5.3943	6.6510
Iter num	-	20	19	6	18	19	25

TABLE IX: Values of the estimated parameters for scaled initialization for image with SNR = 5dB, Nh = 2

VI. Conclusion

The new non-radial vignetting model was introduced in the paper based on a low-order harmonic representation of the angular-dependent vignetting shape. The feasibility of model estimation through non-linear optimization was investigated and the influence of the proper parameter initialization on the estimated model accuracy was evaluated by comparing the estimated model to the synthetic one. The effect of image noise level on reconstruction accuracy was also considered. The presented results are

param	true\ α	1	0.7	0.4	0.2	0	-1
ma_1	0.0466	0.0459	0.0330	0.0175	0.0093	0.0001	-0.0465
ma_2	0.1014	0.1005	0.0709	0.0400	0.0203	0.0002	-0.1018
ma_3	0.0360	0.0371	0.0254	0.0142	0.0072	0	-0.0366
ma_4	0.1408	0.1399	0.0984	0.0559	0.0282	0.0008	-0.1409
ma_5	0.0895	0.0901	0.0626	0.0355	0.0179	0.0002	-0.0896
ma_6	0.0176	0.0144	0.0121	0.0071	0.0035	-0.0004	-0.0180
ma_7	0.1566	0.1560	0.1097	0.0625	0.0313	-0.0005	-0.1564
ma_8	0.0218	0.0219	0.0158	0.0088	0.0044	-0.0008	-0.0219
ma_9	0.0366	0.0368	0.0257	0.0145	0.0073	0.0005	-0.0363
an_1	0.4492	0.4496	0.3148	0.1800	0.0898	0	-0.4484
an_2	0.2998	0.2984	0.2103	0.1191	0.0600	0	-0.2992
an_3	-0.4346	-0.4351	-0.3041	-0.1744	-0.0869	0	0.4350
an_4	-0.0787	-0.0781	-0.0549	-0.0322	-0.0157	0	0.0781
an_5	-0.2185	-0.2181	-0.1530	-0.0876	-0.0437	0	0.2191
an_6	-0.4015	-0.4022	-0.2811	-0.1607	-0.0803	0	0.4019
an_7	-0.0884	-0.0895	-0.0620	-0.0359	-0.0177	0	0.0883
an_8	0.4547	0.4541	0.3184	0.1817	0.0909	0	-0.4545
an_9	-0.0004	-0.0002	-0.0003	-0.0003	-0.0001	0	0.0007
valid %	-	97.850	97.970	98.882	98.677	98.366	98.635
std %	-	1.5375	2.6741	4.3433	5.4530	6.2868	9.4832
Iter num	-	125	60	61	20	60	81

TABLE X: Values of the estimated parameters for scaled initialization for image with SNR = 5dB, Nh = 9

so far limited to the simplified case with a priori known origin of the model. The paper shows that highly accurate models can be estimated especially for a lower number of angular harmonics with residual gain error std of less than 0.03%. Even for images corrupted with 5dB noise the gain error std is still below 3% with proper parameter initialization prior to optimization. Such results are very encouraging and in our future work, the model origin estimation will also be considered, as well as appropriate analytical methods for parameter initialization. The higher-order models with a larger number of angular harmonics are more challenging for estimation as was illustrated for the case with 9 harmonics. The study of non-radial vignetting and its correction provides valuable insights into the nature of vignetting and the potential for new and improved correction methods.

References

[1] Y. Zheng, S. Lin, C. Kambhamettu, J. Yu, and S. B. Kang, "Single-image vignetting correction," *IEEE Transactions on Pattern Analysis and Machine Intelligence*, vol. 31, no. 12, pp. 2243–2256, 2009.

[2] S. J. Kim and M. Pollefeys, "Robust radiometric calibration and vignetting correction," *IEEE Transactions on Pattern Analysis and Machine Intelligence*, vol. 30, no. 4, pp. 562–576, 2008.

[3] A. Kordecki, H. Palus, and A. Bal, "Practical vignetting correction method for digital camera with measurement of surface luminance distribution," *Signal, Image and Video Processing*, vol. 10, pp. 1417 – 1424, 2016.

[4] S. Cushing, "Optical vignetting," https://u42.co/Tech-Blog/Vignetting/Vignetting.html, [Online; accessed 21.12.2022.].

[5] RED-101, "Understanding lens vignetting," https://www.red.com/red-101/lens-vignetting, [Online; accessed 21.12.2022.].

[6] P. Kumar, "What is lens vignetting - and how to eliminate it in embedded cameras?" https://www.e-consystems.com/blog/camera/technology/what-is-lens-vignetting-and-how-to-eliminate-it-in-embedded-cameras/, 2022, [Online; accessed 21.12.2022.].

[7] N. Mansurov, "What is Vignetting," https://photographylife.com/what-is-vignetting, 2020, [Online; accessed 21.12.2022.].

[8] W. Emery and A. Camps, "Optical imaging systems," in *Introduction to Satellite Remote Sensing*. Elsevier, 2017, pp. 85–130. [Online]. Available: https://doi.org/10.1016/b978-0-12-809254-5.00003-8

[9] B. Carnathan, "Sigma 105mm f/1.4 DG HSM Art Lens Review," https://www.the-digital-picture.com/Reviews/Sigma-105mm-f-1.4-DG-HSM-Art-Lens.aspx, 2018, [Online; accessed 20.03.2023.].

[10] N. Asada, A. Amano, and M. Baba, "Photometric calibration of zoom lens systems," in *Proceedings of the 1996 International Conference on Pattern Recognition (ICPR '96) Volume I - Volume 7270*, ser. ICPR '96. USA: IEEE Computer Society, 1996, p. 186.

[11] P. B. Catrysse, X. Liu, and A. E. Gamal, "Qe reduction due to pixel vignetting in cmos image sensors," in *Electronic imaging*, 2000.

[12] T. Rohlfing, "Single-image vignetting correction by constrained minimization of log-intensity entropy," Sep 2012.

[13] Y. Zheng, C. Kambhamettu, and S. Lin, "Single-image optical center estimation from vignetting and tangential gradient symmetry," *2009 IEEE Conference on Computer Vision and Pattern Recognition*, pp. 2058–2065, 2009.

[14] H. Cho, H. Lee, and S. Lee, "Radial bright channel prior for single image vignetting correction," in *Computer Vision – ECCV 2014*, D. Fleet, T. Pajdla, B. Schiele, and T. Tuytelaars, Eds. Cham: Springer International Publishing, 2014, pp. 189–202.

[15] D. B. Goldman and J.-H. Chen, "Vignette and exposure calibration and compensation." USA: IEEE Computer Society, 2005. [Online]. Available: https://doi.org/10.1109/ICCV.2005.249

[16] H. T. Lin, Z. Lu, S. J. Kim, and M. S. Brown, "Nonuniform lattice regression for modeling the camera imaging pipeline," in *Computer Vision – ECCV 2012*, A. Fitzgibbon, S. Lazebnik, P. Perona, Y. Sato, and C. Schmid, Eds. Berlin, Heidelberg: Springer Berlin Heidelberg, 2012, pp. 556–568.

[17] D. B. Goldman, "Vignette and exposure calibration and compensation," *IEEE Transactions on Pattern Analysis and Machine Intelligence*, vol. 32, no. 12, pp. 2276–2288, 2010.

[18] C. Doutre and P. Nasiopoulos, "Fast vignetting correction and color matching for panoramic image stitching," *2009 16th IEEE International Conference on Image Processing (ICIP)*, pp. 709–712, 2009.

[19] S. B. Kang and R. Weiss, "Can we calibrate a camera using an image of a flat, textureless lambertian surface?" in *Lecture Notes in Computer Science*. Springer Berlin Heidelberg, 2000, pp. 640–653. [Online]. Available: https://doi.org/10.1007/3-540-45053-x_41

[20] K. He, P.-F. Tang, and R. Liang, "Vignetting image correction based on gaussian quadrics fitting," in *2009 Fifth International Conference on Natural Computation*, vol. 5, 2009, pp. 158–161.

[21] D. Zhang, Q. Y. Yang, and T. Chen, "Vignetting correction for a single star-sky observation image," *Applied Optics*, vol. 58, no. 16, p. 4337, May 2019. [Online]. Available: https://doi.org/10.1364/ao.58.004337

[22] M. Aggarwal, H. Hua, and N. Ahuja, "On cosine-fourth and vignetting effects in real lenses," in *Proceedings Eighth IEEE International Conference on Computer Vision. ICCV 2001*, vol. 1, 2001, pp. 472–479 vol.1.

[23] Y. Zheng, J. Yu, S. B. Kang, S. Lin, and C. Kambhamettu, "Single-image vignetting correction using radial gradient symmetry," in *2008 IEEE Conference on Computer Vision and Pattern Recognition*, 2008, pp. 1–8.

[24] A. A. Sawchuk, "Real-time correction of intensity nonlinearities in imaging systems," *IEEE Transactions on Computers*, vol. C-26, no. 1, pp. 34–39, 1977.

[25] M. Brady and G. Legge, "Camera calibration for natural image studies and vision research," *Journal of the Optical Society of America A: Optics and Image Science, and Vision*, vol. 26, no. 1, pp. 30–42, Jan. 2009.

[26] A. Bal and H. Palus, "A smooth non-iterative local polynomial (snilp) model of image vignetting," *Sensors*, vol. 21, no. 21, 2021. [Online]. Available: https://www.mdpi.com/1424-8220/21/21/7086

[27] P. J. Burt and E. H. Adelson, "A multiresolution spline with application to image mosaics," *ACM Transactions on Graphics (TOG)*, vol. 2, no. 4, pp. 217–236, 1983.

[28] W. Yu, "Practical anti-vignetting methods for digital cameras," *IEEE Trans. Consumer Electron.*, vol. 50, pp. 975–983, 2004.

[29] F. J. W.-M. Leong, M. Brady, and J. O. McGee, "Correction of uneven illumination (vignetting) in digital microscopy images," *Journal of Clinical Pathology*, vol. 56, no. 8, pp. 619–621, 2003. [Online]. Available: https://jcp.bmj.com/content/56/8/619

[30] A. Bal and H. Palus, "Image vignetting correction using a deformable radial polynomial model," *Sensors*, vol. 23, no. 3, p. 1157, 2023.

[31] A. Kordecki, A. Bal, and H. Palus, "Local polynomial model: A new approach to vignetting correction," in *Ninth International Conference on Machine Vision (ICMV 2016)*, vol. 10341. SPIE, 2017, pp. 463–467.

[32] D. Potoč; and D. Petrinović;, "Creating a synthetic image for evaluation of vignetting modeling and estimation," in *2022 45th Jubilee International Convention on Information, Communication and Electronic Technology (MIPRO)*, 2022, pp. 918–923.